SIMPLE DESIGN EQUATIONS FOR OMNIDIRECTIONAL AXIS-DISPLACED DUAL-REFLECTOR ANTENNAS

José R. Bergmann[1] and Fernando J. S. Moreira[2]
[1] CETUC–Center for Telecommunications Studies
Catholic University of Rio de Janeiro
Rio de Janeiro, RJ 22453-900, Brazil
[2] Department of Electronics Engineering
Federal University of Minas Gerais
Belo Horizonte, MG 30161-970, Brazil

Received 14 October 2004

ABSTRACT: *This paper considers the use of dual-reflector antennas for omnidirectional coverage. The reflectors are axially symmetric surfaces generated by axis-displaced conic sections. By using geometrical optics (GO) principles, simple design equations for the different configurations are established. The simple equations allow an easy identification of the relevant features of the different dual-reflector configurations. The design parameters are explored to provide compact arrangements suited for use at base stations of point-to-multi-point radio links. The design for maximum efficiency is obtained by employing a combination of GO fields and an aperture method to evaluate the antenna-radiation patterns. Numerical simulations based on the method of moments (MoM) are presented to illustrate the usefulness and advantages of the proposed dual-reflector antennas.* © 2005 Wiley Periodicals, Inc.
Microwave Opt Technol Lett 45: 159–163, 2005; Published online in Wiley InterScience (www.interscience.wiley.com). DOI 10.1002/mop.20756

Key words: *dual reflector antennas; omnidirectional antennas*

1. INTRODUCTION

Reflector antennas can yield compact designs capable of providing the wide bandwidth required to operate broadband wireless access services at Ka and millimeter waves. For vertical polarization and omnidirectional coverage in the aximuthal plane, several design examples of circularly symmetric single- and dual-reflector antennas have been presented [1–5]. The case of a dual-reflector antenna with a paraboloidal subreflector and conical main reflector has been investigated in [2, 3], in which the feed return loss brought by the strong feed-subreflector interaction may arouse concerns, especially when designing for compact reflector arrangements. To reduce the feed return loss, a reflector system based on the axis-displaced ellipse (ADE) configuration has been proposed [5], which consists of circularly symmetric subreflectors and main reflectors generated by an ellipse and a parabola, respectively. One of the major features of the omnidirectional ADE (OADE) is the presence of a real-ring caustic between the reflectors, which can be set to minimize the subreflector radiation toward the feed horn (thus reducing the feed return loss) while enabling a larger aperture width with relatively smaller reflector diameters (which is desirable for compact-antenna applications).

In this paper, we explore the design of general classical axis-displaced dual-reflector antennas for omnidirectional coverages. By using geometrical optics (GO) principles, we derive simple closed-form expressions for their design and the identification of their geometrical properties. GO is also used to obtain closed-form equations for the vector field at the antenna cylindrical aperture, following the procedure of Westcott et al. [6]. The GO aperture field is then used to estimate the antenna gain by employing the aperture method. The above procedure is applied to identify the antennas providing higher efficiencies and compact geometries. To validate the procedure, two design examples are analyzed using the method of the moments (MoM).

This work was partially supported by CNPq under Covenant PRONEX 664041/1996-S and project nos. 462669/00-9, 470495/2001-4, and 551990/2002-2, and by FAPEMIG under project no. TEC 659/98.

2. DUAL REFLECTOR GEOMETRIES FOR OMNIDIRECTIONAL COVERAGE

In the classical axis-displaced dual-reflector configurations for directive antennas, the circularly symmetric reflectors are yielded by the rotation of conic sections about a symmetry axis [7]. The rays reflected from the main reflector are parallel to the symmetry axis, thus creating a uniform phase front at the aperture plane [7]. Alternatively, to obtain omnidirectional coverage, the axis of the main-reflector parabolic section is tilted by 90° such that the rays reflected by the main reflector will be orthogonal to the antenna-symmetry axis, thus creating a cylindrical wave front. Figures 1 and 2 illustrate the vertical plane of the omnidirectional dual-reflector configurations (hereinafter named mapping options I and II, respectively), with a subreflector generated by an ellipse or hyperbola and a main reflector generated by a parabola. One of the ellipse/hyperbola foci O is placed at the symmetry axis, defining the focus of the dual-reflector system. The other focus P_0 coincides with the parabola focus and will define a ring caustic after the rotation of the generating conics about the symmetry axis z. The main reflector has a small circular central aperture (with radius R_B), which enables the feed to have access to the focal point O.

In order to achieve an omnidirectional dual-reflector system in a unique manner, five parameters must be specified: (i) the parabola focal length f_P, (ii) the ellipse/hyperbola eccentricity e, (iii) the interfocal distance $2c$, (iv) the angle (γ) between the ellipse/hyperbola and the parabola axes, and (v) the subreflector edge angle θ_E. As these are not appropriate input parameters for practical designs, five other parameters are chosen instead (see Figs. 1 and 2): the distance V_S from O to the subreflector vertex Q, the radii of the main-reflector inner R_B and outer R_M rims, the width W_A of the antenna cylindrical aperture, and the z coordinate of the main-reflector central aperture Z_B.

To describe the design procedure of the dual-reflector omnidirectional antennas in a simple way, we adopt the auxiliary angles α and β, defined with the help of the coordinates of the main-reflector points as follows:

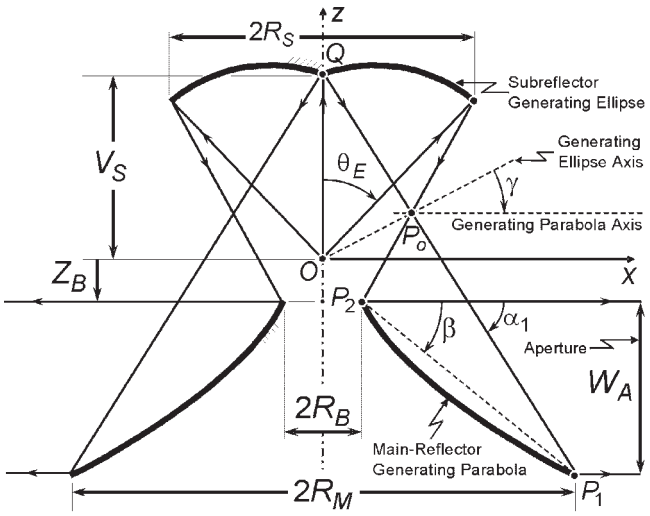

Figure 1 Antenna geometry and basic parameters for mapping option I (here, an OADE).

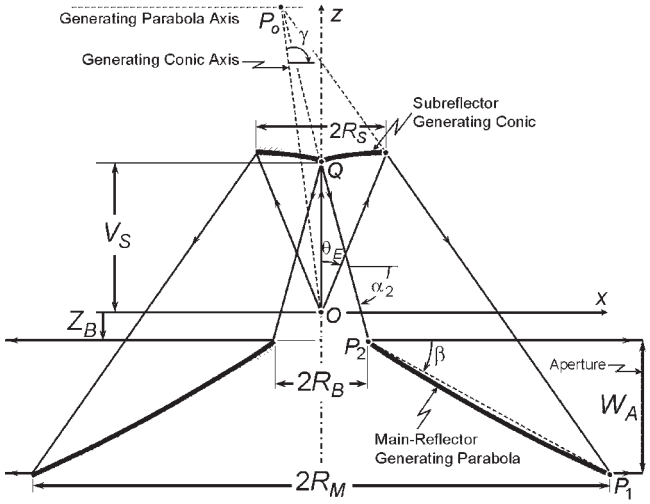

Figure 2 Antenna geometry and basic parameters for mapping option II (here, an OADC)

$$P_1(x_1 = R_M,\ z_1 = z_B - W_A) \quad \text{and} \quad P_2(x_2 = R_B,\ z_2 = z_B), \tag{1}$$

according to Figures 1 and 2 (note that the origin is at O). β is the angle that $\overline{P_2P_1}$ makes with the x axis, given by

$$\tan\beta = \frac{W_A}{R_M - R_B}. \tag{2}$$

The main difference between the two mapping options is characterized by the "reflection" of the feed principal ray (along the z axis) from the subreflector vertex Q. For the mapping option I (depicted in Fig. 1) the principal ray is reflected toward P_1, while for option II (Fig. 2) it is directed toward P_2. Consequently, option I provides the inversion of the feed illumination at the antenna cylindrical aperture, which does not occur for option II. The corresponding angle α_i that such a reflected ray makes with the x axis is given by

$$\tan\alpha_i = \frac{V_S - z_i}{x_i}, \tag{3}$$

where x_i and z_i are the coordinates of P_i, according to Eq. (1). Hereinafter the subscript i will be used to identify the antenna mapping options ($i = 1$ or 2 for options I or II, respectively).

The design procedure imposes P_1 and P_2 at the parabola section with focus at P_0 (see Figs. 1 and 2). From the parabola equation one can show that the distance (V_{0i}) from P_0 to P_i is given by

$$V_{0i} = \frac{\pm W_A}{2}\left[\frac{\sin\beta}{\cos(\alpha_i - \beta) - \cos\beta}\right], \tag{4}$$

where the $\pm$ sign refers to mapping option I (II), and that the parabola focal distance is given by

$$f_P = \frac{V_{0i}}{2}(1 - \cos\alpha_i). \tag{5}$$

From Eq. (4) and Figures 1 and 2, one can also determine the coordinates of P_0 as follows:

$$x_0 = x_i - V_{0i}\cos\alpha_i \quad \text{and} \quad z_0 = z_i + V_{0i}\sin\alpha_i, \tag{6}$$

from which the ellipse/hyperbola parameters are further obtained:

$$2c = \sqrt{x_0^2 + z_0^2}, \tag{7}$$

$$\tan\gamma = \frac{z_0}{x_0}, \tag{8}$$

$$\frac{2c}{e} = V_S + \frac{x_0}{\cos\alpha_i}. \tag{9}$$

With the conic parameters established, the reflector surfaces are uniquely determined for each mapping option.

3. GEOMETRICAL FEATURES

The geometrical features of the omnidirectional dual-reflector antennas are explored in this section. We first notice that the relation between β and α_i, given by Eqs. (2) and (3), respectively, defines whether V_{0i} in Eq. (4) is positive or negative and, consequently, the position of the ring caustic defined by P_0 (x_0, z_0), as observed from Eq. (6). For instance, for the mapping option I (II), $\alpha_1 < 2\beta$ ($\alpha_2 > 2\beta$) provides a positive-valued f_P (that is, $V_{0i} > 0$) and, consequently, a concave generating parabola (that is, P_0 is "above" the main-reflector surface, as depicted in Figs. 1 and 2). Otherwise, the parabola is convex. The turning point corresponds to $\alpha_i = 2\beta$, when $|V_{0i}| \to \infty$ and, consequently, $|z_0| \to \infty$.

In particular, the position of P_0 defines the dual-reflector configuration among the four identified in [7]. If P_0 lies between the subreflector and the main reflector, then the corresponding ring caustic is real and the antenna is either an omnidirectional ADE (for the mapping option I, as depicted in Fig. 1) or ADG (axis-displaced Gregorian, for option II). Otherwise, the ring caustic is virtual and we have an omnidirectional ADH (axis-displaced hyperbola, for option I) or ADC (axis-displaced Cassegrain, for option II, as depicted in Fig. 2). So, each mapping option is associated with two different antenna configurations. Now, the turning point occurs for $P_0 \to Q$, when both the subreflector edge angle θ_E and its rim radius R_S tend to zero (see Figs. 1 and 2). It is then useful to define an auxiliary angle α_T in order to identify the two different configurations of a mapping option. α_T is established by setting $x_0 = 0$ in Eq. (6) as follows:

$$\tan\frac{\alpha_T}{2} = \frac{\pm W_A}{2x_i - \sqrt{W_A^2 + 4R_MR_B}}, \tag{10}$$

where the $\pm$ sign refers to mapping option I (II). If $\alpha_i < \alpha_T$, then the antenna is an omnidirectional ADE (OADE) or ADC (OACD) for mapping options I or II, respectively. If $\alpha_i > \alpha_T$, we obtain an omnidirectional ADH (OADH) or ADG (OADG) for options I or II, respectively.

As reference for a comparative study, we consider antenna designs with $W_A = 10\lambda$, $R_B = 1\lambda$, and $z_B = 0$ (that is, O is at the main-reflector central aperture of Figs. 1 and 2). The antenna geometries are obtained by varying the remaining input parameters V_S and R_M. In the following plots, the lowest value of V_S for each curve is determined to avoid subreflector blockage of the antenna cylindrical aperture, which occurs for $\theta_E > 90°$ when $z_B = 0$ (see Figs. 1 and 2).

We start by presenting the values of θ_E and R_S shown in Figures 3(a) and 3(b), respectively, for the mapping option I. These values can be obtained by applying the sine law to the triangle

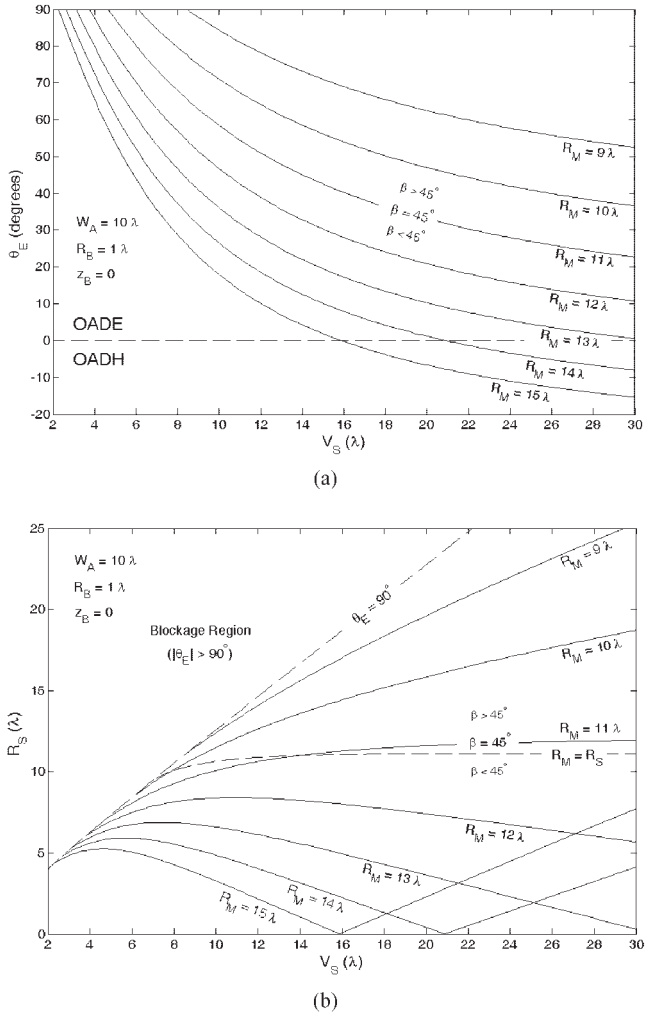

Figure 3 Values of (a) θ_E and (b) R_S as functions of V_S and R_M for mapping option I

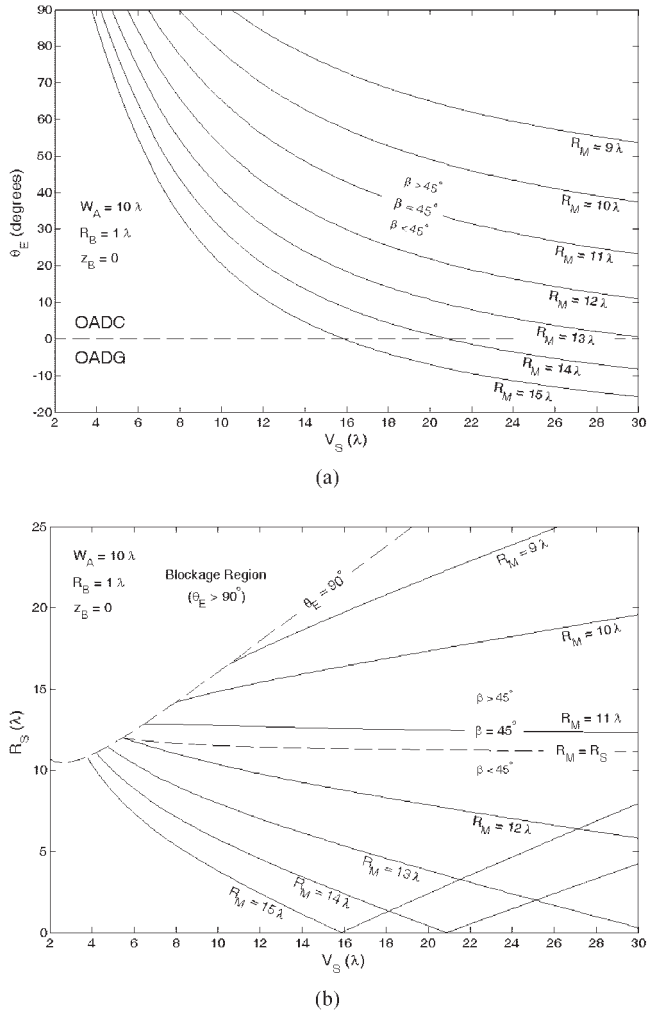

Figure 4 Values of (a) θ_E and (b) R_S as functions of V_S and R_M for mapping option II

ORP_0 in Figure 1. θ_E and R_S, together with the input parameters, are useful in determining compact reflector arrangements. In Figure 3(a), positive θ_E values correspond to OADE antennas (that is, $\alpha_1 < \alpha_T$), while the negative ones correspond to OADH configurations ($\alpha_1 > \alpha_T$). Note that $\theta_E = 0$ in Figure 3(a) matches $R_S = 0$ in Figure 3(b), as anticipated. From Eq. (2) we observe that β does not depend on V_S. So, the curves for constant R_M also correspond to constant β ($R_M = 11\lambda$ corresponds to $\beta = 45°$ for the present antennas). For $\beta > 45°$ (that is, $R_M < 11\lambda$), Figure 1 and Eqs. (4) and (6) indicate that V_{01} and x_0 are always positive and, consequently, the antenna is an OADE (that is, $\alpha_1 < \alpha_T$ when $\beta > 45°$), with an ellipse and a concave parabola generating the subreflector and the main reflector, respectively. For $\beta < 45°$, the antenna may be an OADE ($\alpha_1 < \alpha_T$) or an OADH ($\alpha_1 > \alpha_T$). For the OADE, we note from Figure 3(b) that R_S reaches a maximum value for a fixed R_M, thus indicating that the distance V_S between the feed and subreflector can be slightly adjusted when necessary without compromising a desirable compact reflector arrangement. As V_S increases, the configuration eventually becomes an OADH, for which the subreflector and main reflector are initially generated by a hyperbola and a concave parabola (that is, $\alpha_T < \alpha_1 < 2\beta$). However, as V_S keeps increasing, $\alpha_1 \to 2\beta$ and $z_0 \to \infty$. After that, $\alpha_1 > 2\beta$ and P_0 appears "below" the main reflector (the generating parabola becomes convex and the subreflector is generated by an ellipse).

When aiming for compact reflector arrangements, one should aim for smaller V_S values. According to Figure 3(b), R_S increases as R_M decreases. So, the optimum choice for compact arrangements should have $R_S \approx R_M \approx W_A$ (that is, $\beta \approx 45°$, as usually

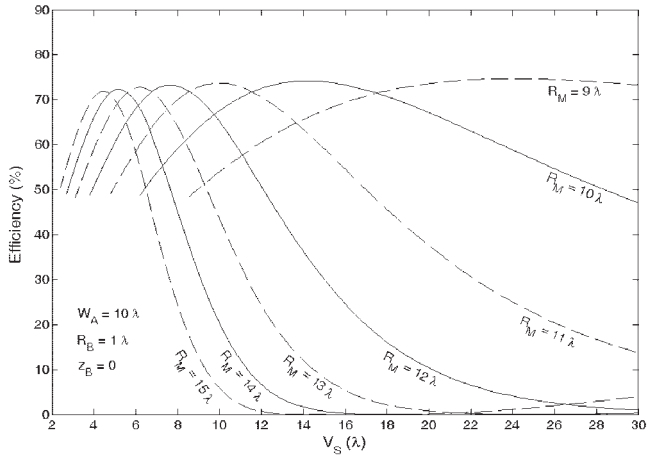

Figure 5 Antenna efficiency as a function of V_S and R_M for mapping option I

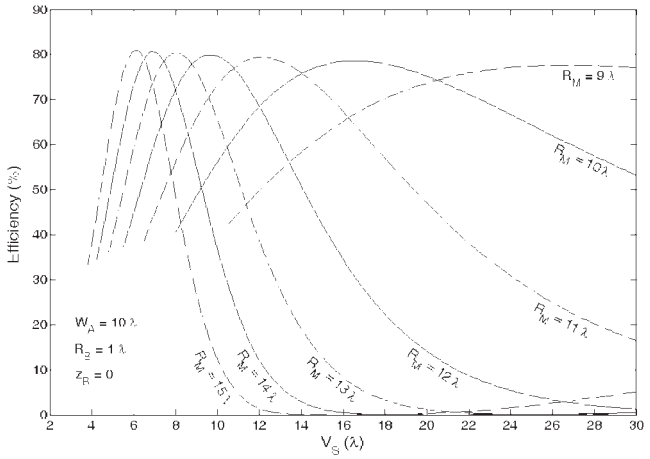

Figure 6 Antenna efficiency as a function of V_S and R_M for mapping option II

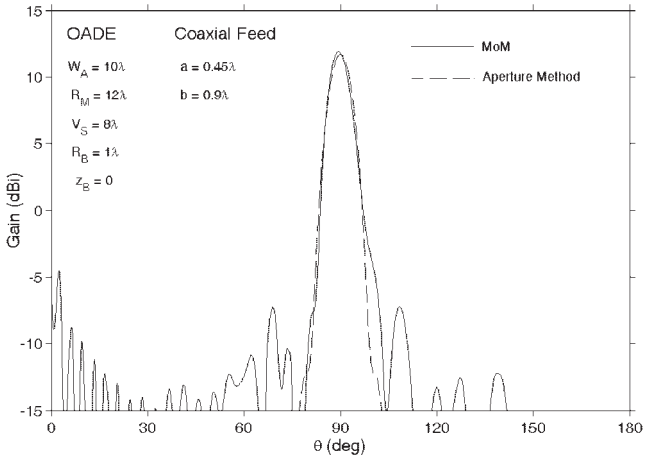

Figure 7 OADE radiation pattern evaluated by MoM (solid line) and aperture method (dashed line)

$R_B \ll R_M$), necessarily an OADE. The dashed $R_M = R_S$ curve in Figure 3(b) helps to visualize such choice.

The values of θ_E and R_S for the mapping option II are depicted in Figures 4(a) and 4(b), respectively. As inspected from Figures 3(a) and 4(a), the behavior of θ_E is basically the same for both mapping options. Now, positive values of θ_E (that is, $\alpha_2 < \alpha_T$) correspond to OADC configurations (otherwise, the antenna is an OADG). For $\beta > 45°$ (that is, $R_M < 11\lambda$), the antenna is always an OADC with a hyperbola and a convex parabola generating the subreflector and main reflector, respectively (that is, $\alpha_2 < \alpha_T$ and $\alpha_2 < 2\beta$ when $\beta > 45°$). For $\beta < 45°$ the antenna is either an OADC ($\alpha_2 < \alpha_T$) or an OADG ($\alpha_2 > \alpha_T$). As V_S increases, the first turning point occurs for $\alpha_2 = 2\beta$. After that (that is, $2\beta < \alpha_2 < \alpha_T$) P_0 is "above" the subreflector and the OADC has a concave parabola. The second turning point occurs for $\alpha_2 = \alpha_T$ (that is, $P_0 = Q$). For $\alpha_2 > \alpha_T$, the antenna becomes an OADG with an ellipse and a concave parabola generating the subreflector and main reflector, respectively. As for the previous mapping option, compact reflector arrangements are yielded by $R_S \approx R_M \approx W_A$ and, consequently, $\beta = 45°$ [see Fig. 4(b)]. Finally, it is interesting to observe that the antennas investigated in [2, 3] are OADCs with $R_B = 0$ (the subreflector is a paraboloid and the main reflector is a cone).

4. ANTENNA RADIATION MODEL

For the present investigation, the feed is represented by the θ-polarized rotationally symmetric electric field radiated by a coaxial aperture illuminated by the TEM mode, given by [3]:

$$\tilde{E}_F = V(\theta_F)\,\frac{\exp(-jkr_F)}{r_F}\,\hat{\theta}_F, \tag{11}$$

where the subscript F identifies the feed coordinate system (with origin at O and the z axis, as indicated in Figs. 1 and 2) and

$$V(\theta_F) = E_0\left[\frac{J_0(ka\,\sin\theta_F) - J_0(kb\,\sin\theta_F)}{\sin\theta_F}\right], \tag{12}$$

where J_0 is the Bessel function of order zero and a and b are the inner and outer radii of the coaxial aperture, respectively (note that $a < b < R_B$). In the GO sense, the rays emanating from O in the direction θ_F, after two reflections, cross the antenna cylindrical aperture at a point with $z = z_A$. Following the procedure in [6], for a uniform phase at the cylindrical aperture, the relation between θ_F and z_A for both mapping options is given by

$$\eta_F = \cot\frac{\theta_F}{2} = \frac{c_1 + c_2 + (d_2 - c_2)(z_A/\ell_o)}{c_1 - c_2 - (d_2 + c_2)(z_A/\ell_o)}, \tag{13}$$

where $\ell_o = V_{0i} - x_i + 2c/e$ is the constant optical path from O to the symmetry axis z, $c_1 = e\cos\gamma + 1 - 2c(1 - e^2)/(\ell_o e)$, $c_2 = e\sin\gamma$, and $d_2 = e\cos\gamma - 1$ [6]. It is important to note that in Eq. (13) θ_F is negative for the OADH and OADG (that is, for $\alpha_i > \alpha_T$). By applying energy conservation and GO principles, the TEM field at the cylindrical aperture, apart from a constant-phase term, is given by [6]:

TABLE 1 Geometrical Characteristics of the Antennas with Maximum Efficiency as Functions of R_M, with $W_A = 10\lambda$, $R_B = 1\lambda$, and $z_B = 0$

	Mapping Option I (OADE)					Mapping Option II (OADC)				
R_M [λ]	V_S [λ]	R_S [λ]	θ_E [°]	Vol. [λ³]	Eff. [%]	V_S [λ]	R_S [λ]	θ_E [°]	Vol. [λ³]	Eff. [%]
9	24.1	22	57.7	52250	74.7	26.6	25.2	56.6	73100	77.7
10	14.2	13.7	58	14400	74.2	16.6	16.6	55.9	22900	78.6
11	10	10.1	58.4	7720	73.7	12.2	12.7	55.2	11200	79.4
11.5	8.7	8.9	58.6	7900	73.5	10.7	11.5	55	8630	79.7
12	7.7	8.1	58.8	8150	73.2	9.6	10.5	54.8	8900	80
13	6.2	6.8	59.1	8800	72.8	8.1	9.1	54.2	9600	80.4
14	5.2	5.9	59.6	9570	72.3	6.9	8	54	10450	80.7
15	4.5	5.2	59.7	10500	71.9	6.1	7.3	52.9	11425	80.9

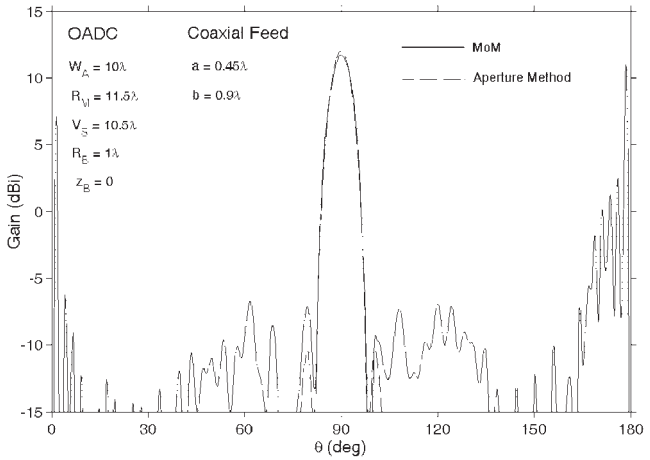

Figure 8 OADC radiation pattern evaluated by MoM (solid line) and aperture method (dashed line)

$$\vec{E}_A = \pm V(\theta_F)\left|\frac{d_2 - c_2 + (d_2 + c_2)\eta_F}{1 + \eta_F^2}\right| \sqrt{\frac{|\eta_F|}{|f_P(1 - e^2)|}}\,\hat{z}, \quad (14)$$

where the $\pm$ sign refers to the OADH or OADG (OADE or OADC). The antenna far-field radiation is then obtained by integrating the GO aperture field (aperture method). The aperture stop is simply specified by $0 \le |\theta_F| \le |\theta_E|$, with the help of Eq. (13).

As the cylindrical aperture has a uniform phase distribution (according to GO), the far-field peak occurs at $\theta = 90°$. The corresponding directivity D_o is compared against the maximum directivity $D_{\max}$—given by Eq. (11) of [3]—of a uniform cylindrical aperture with the same dimensions and radiating the same feed power. The antenna efficiency is then defined by the ratio $D_o/D_{\max}$, thus accounting for both illumination and spillover efficiencies. Figures 5 and 6 illustrate the antenna efficiencies obtained for mapping options I and II, respectively, as functions of V_S and R_M (still with $W_A = 10\lambda$, $R_B = 1\lambda$, and $z_B = 0$). The efficiencies were obtained by the aperture method, with the help of Eqs. (11)–(14) with $a = 0.45\lambda$ and $b = 0.9\lambda$. As observed in those figures, the antenna efficiency strongly depends on V_S and its maximum is obtained by compromising spillover losses (note that θ_E decreases as V_S increases, increasing the subreflector spillover) and the uniform illumination of the aperture. Note that in Figures 5 and 6 the designs with maximum efficiencies correspond to OADE and OADC configurations, respectively.

From Figures 5 and 6 one can also observe that R_M does not significantly affect the maximum efficiency; however, it does affect the antenna size. Table 1 compares the antenna volumes (defined by the cylinder that circumscribes the dual-reflector system) obtained for the designs with maximum efficiency, according to Figures 5 and 6. As anticipated in section 2, the minimum volume occurs for $R_M \approx W_A$ and, consequently, $\beta \approx 45°$ for both mapping options. For $\beta < 45°$ the volume approximately grows with R_M^2, although V_S decreases. For $\beta > 45°$, the volume grows faster, as R_S drastically increases while R_M decreases.

To validate the previous procedure and show its usefulness, MoM analyses were conducted to evaluate of the radiation patterns of two representative antennas: an OADE with $R_M = 12\lambda$ and $V_S = 8\lambda$, and an OADC with $R_M = 11.5\lambda$ and $V_S = 10.5\lambda$, as depicted in Figures 7 and 8, respectively. The main-beam characteristics yielded by the aperture method show good agreement with those of the MoM analyses. The aperture method predicts gains of 11.7 and 12 dBi for the OADE and OADC, respectively, while the MoM estimates 11.9 and 11.7 dBi, respectively. The small discrepancies between the different methods (about ± 0.3-dB in gain) is due to the strong electromagnetic coupling between the reflector surfaces of such compact arrangements.

5. CONCLUSION

This paper has considered the classical dual reflector for omnidirectional coverage using geometrical optics (GO) principles to obtain simple closed-form equations for the geometry design and for the vector field at the antenna cylindrical aperture. Main-beam radiation characteristics were estimated by integrating the GO aperture field (the aperture method). This procedure allows a parametric study to identify the geometrical and radiation features of different types of dual-reflector configurations. The OADE and OADC were chosen for compromising higher efficiencies and compactness. For these two configurations, the antenna performance yielded by the formulation presented in this work was compared against MoM analyses, showing good agreement for antennas with aperture widths $W_A = 10\lambda$ or larger.

REFERENCES

1. A.P. Norris and W.D. Waddoup, A millimetric wave omnidirectional antenna with prescribed elevation shaping, Proc 4th Int Conf Antennas Propagat (ICAP), 1985, pp. 141–145.
2. M. Orefice and P. Pirinoli, Dual reflector antenna with narrow broadside beam for omnidirectional coverage, Electron Lett 29 (1993), 2158–2159.
3. A.G. Pino, A.M.A. Acuña, and J.O.R. Lopez, An omnidirectional dual-shaped reflector antenna, Microwave Opt Technol Lett 25 (2000), 371–374.
4. J.R. Bergmann, F.J.V. Hasselmann, and M.G.C. Branco, A single-reflector design for omnidirectional coverage, Microwave Opt Technol Lett 24 (2000), 426–429.
5. J.R. Bergmann and F.J.S. Moreira, An omnidirectional ADE reflector antenna, Microwave Opt Technol Lett 40 (2004), 250–254.
6. B.S. Westcott, F.A. Stevens and F. Brickell, GO synthesis of offset dual-reflectors, IEE Proc 128 H (1981), 11–18.
7. F.J.S. Moreira and A. Prata, Jr. Generalized classical axially symmetric dual-reflector antennas, IEEE Trans Antennas Propagat 49 (2001), 547–554.

A NOVEL ELECTRONICALLY SCANNABLE LOG-PERIODIC LEAKY-WAVE ANTENNA

Gijo Augustin, S. V. Shynu, C. K. Aanandan, P. Mohanan, and K. Vasudevan
Centre for Research in Electromagnetics and Antennas
Department of Electronics
Cochin University of Science and Technology
Cochin 682 022, India

Received 4 October 2004

ABSTRACT: *An innovative phaseshifterless, wideband, microstrip leaky-wave antenna with an electronically steerable dual-pencil-beam pattern in the H-plane is presented. The log-periodic geometry of the leaky slots of the antenna results in a wide bandwidth of 25.19%. The fan beam can be steered up to 14° over the wide resonating band of the antenna. The beam is also steerable at a fixed frequency, by reactivelty loading the slots and a maximum steering angle of about 14° is observed for different capacitor values with an improved bandwidth of 33.3%. This concept is studied using passive components, but it can be*